Pergamon

Geochimica et Cosmochimica Acta, Vol. 59, No. 18, pp. 3671–3683, 1995

0016-7037/95 $9.50 + .00

0016-7037(95)00270-7

Selected trace and minor element partitioning between peridotite minerals and carbonatite melts at 18–46 kb pressure

R. J. SWEENEY,[1] V. PROZESKY,[2] and W. PRZYBYLOWICZ[2,*]

[1] Institute fur Mineralogie und Petrographie, ETH Zurich, Sonneggstr. 5, CH-8092, Zurich, Switzerland
[2] Van de Graaff Group, National Accelerator Centre, P.O. Box 72, Faure 7131, South Africa

(*Received August* 22, 1994; *accepted in revised form June* 9, 1995)

Abstract—Analysis of silicate minerals equilibrated at high pressure with silicate- (clinopyroxene) and carbonatite-melts (olivine, orthopyroxene, clinopyroxene, garnet, phlogopite) using proton- and electron-microprobe techniques, enabled the measurement of single mineral/melt partition coefficients for elements in minor and trace abundances. For carbonatite melt—olivine (18 kb), D_{Ti} (<0.05), D_{Nb} (0.034), D_{Zr} (0.036), D_{Ta} (<0.06), D_{Y} (<0.03), D_{Sr} (0.02); carbonatite melt-orthopyroxene (46 kb), D_{Ti} (0.13) D_{Nb} (<0.01), D_{Zr} (0.17), D_{Ta} (<0.01), D_{Y} (0.18), D_{Lu} (0.52), D_{Sr} (0.053); carbonatite melt-garnet (34 and 46 kb), D_{Ti} (1.2–0.99), D_{Nb} (0.086–0.014), D_{Zr} (1.42–0.83), D_{Ta} (0.14–.051), D_{Y} (1.91–1.53), D_{Lu} (5.3), D_{Sr} (0.062–0.008); carbonatite melt-clinopyroxene (46 kb), D_{Ti} (0.12), D_{Nb} (0.22), D_{Zr} (0.29), D_{Ta} (0.22), D_{Y} (0.27), D_{Lu} (0.33), D_{Sr} (0.26), and carbonatite melt-phlogopite (18 kb), D_{Ti} (2.1) D_{Nb} (0.09), D_{Zr} (0.05), D_{Ta} (0.21), D_{Y} (<0.04), D_{Sr} (0.056), and D_{Rb} (4.0). The partition coefficients are consistent with substitutions involving the main stoichiometric cations Mg, Ca, Fe, and K (phlogopite) in minerals. The effect of different D's and the trace element content of metasomatizing carbonatite and silicate melts will dictate the extent to which trace element ratios may be fractionated differently in residual mantle mineralogies by these two styles of metasomatism. The effect of partitioning differences is quantified using a model assuming equivalent abundances of incompatible minor and trace elements in silicate and carbonatite melts. This model shows that Ti/Na, Ti/Y, Ti/Lu, Ti/Nb, Ti/Ta, and Ti/Sr ratios would be lower in a peridotite affected by carbonatite metasomatism and therefore, in silicate melts derived from such a mantle, relative to a source affected by silicate metasomatism. From natural data (peridotite and carbonatite), element abundances in the metasomatizing carbonatite will also lower these ratios in residual minerals. In addition, the natural data show that carbonatite metasomatism would also increase LREE/HREE, LREE/Hf, LREE/Ti, and Sr/Hf ratios in residual mantle minerals.

1. INTRODUCTION

The equilibration of mantle mineralogies with silicate or carbonatite melts may fractionate trace elements in the mantle in distinctively different ways. To address this question in this study, we present new experimental data obtained in high pressure experimental studies to quantify the manner in which selected trace elements (Rb, Ba, Na, K, Nb, Ta, Sr, Zr, Ti, Y, Lu, Cr) may distribute between carbonate melt and olivine, orthopyroxene, garnet, clinopyroxene, and phlogopite. Some additional measurements are also reported for the partitioning of these elements between silicate melt and garnet and clinopyroxene.

The bulk systems used are listed in Table 1 and are divided into carbonate dominated and silicate-compositions. The silicate bulk systems are the quartz tholeiite (eclogitic) composition of Ringwood and Green (1966) and a kimberlite-borne MARID xenolith composition (AJE137, Waters, 1987). The eclogitic bulk composition may be relevant for any partial fusion of a subducting slab and the MARID composition may represent a small degree mantle melt crystallized at high pressures (Sweeney et al., 1993). In major element terms (SiO_2–Al_2O_3–CaO–MgO–FeO) the variations between the two carbonate systems studied are not significantly different. The major element compositions of the crystallizing phases in the carbonate dominated bulk systems are peridotitic (Sweeney, 1994) and relevant to mineral-melt partitioning in a peridotite where the melt is present in small degrees.

The partition coefficient (D) data obtained for carbonatite melts is compared with available published data in the case of garnet and clinopyroxene. The D's obtained for olivine-, orthopyroxene-, and phlogopite-carbonatite melts are new data. The internal consistency of the partition coefficient data obtained describing carbonatite melt-mineral partitioning is considered in the light of possible ionic substitutions for stoichiometric components in mineral phases. We examine the relative effects of carbonatite and silicate metasomatism on the chemistry of any subsequent melts generated in metasomatized portions of the mantle and then examine the extent to which the chemical consequences of carbonatite metasomatism for a peridotite residue is distinguishable from silicate metasomatism on the basis of partition coefficient differences alone. The evidence for the interaction of carbonatite melts in natural peridotites is reviewed and the effect of element abundance levels in the metasomatizing melt is compared with interelement fractionations caused by differences in D of the residual peridotite minerals.

2. EXPERIMENTAL METHODS

The silicate bulk compositions in Table 1 were made using Na, K, Ba, and Sr added as carbonates, and the remainder as oxides. These were fired at 1000°C and then Fe added as presynthesized fayalite,

* On leave from Faculty of Physics and Nuclear Techniques, Academy of Mining and Metallurgy, Cracow, Poland.

Table 1 Experimental bulk compositions. Mg# is atomic 100*Mg/(Mg+Fe).

	Silicate		Carbonate	
wt%	1	2	3	4
SiO2	44.51	50.38	12.73	10.24
TiO2	2.66	1.76	1.05	0.60
Al2O3	7.97	14.07	3.48	2.20
Cr2O3	0.09	0.07	0.21	0.32
FeO	5.68	10.40	5.52	4.02
MnO		0.11	0.02	
MgO	21.53	7.70	16.79	16.26
CaO	4.23	9.14	18.63	20.46
Na2O	0.90	2.72	4.44	0.40
K2O	7.79	0.00	2.13	4.04
P2O5	0.16	0.19	0.41	0.44
NiO	0.52	0.04	0.06	
Cl	0.35			0.25
F	0.06			0.33
H2O	3.53	3.44	0.85	2.12
total	100.00	100.00	66.32	61.68
Mg#	87.1	56.9	84.4	87.8
ppm				
Nb	1581	2804	1810	1347
Zr	2045	2988	873	1752
Ta	876	2896		874
Ce	3875	4137	3038	4238
Nd	634	2298	437	662
Y	1072	2551		1028
Lu	484	2229		518
Sr	7356	2984	10350	7582
Ba	2935	3161	1893	3778
Pb			76	

1 AJE137 (synthetic) MARID xenolith composition doped with trace elements in ppm.

2 Quartz tholeiite (Ringwood and Green, 1966).

3 Sodic carbonatite composition. Contains ca. 30% CO_2 as carbonate.

4 Potassic carbonatite composition. Contains ca. 37% CO_2 as carbonate.

Cl as $CaCl_2$, F as MgF_2, and H_2O as $Mg(OH)_2$. The addition of H_2O as brucite enabled water to be added in accurate amounts. The carbonatite compositions were synthesized in a similar fashion except that Mg and Ca were added as carbonates and the mix was not fired at 1000°C. The sodic carbonatite bulk composition was composed of 33 wt% of finely ground (<10 μm) of natural AJE137 (MARID) whole-rock powder and 77 wt% of carbonatite composition of Wallace and Green (1988) (see Sweeney, 1994).

The experimental parameters are summarized in Table 2. Partial dissolution of the AgPd alloy used as capsule material by carbonate melt also enabled Ag and Pd partitioning measurements to be made. The experiment mc7 (18 kb) was conducted in a Boyd and England (1960) -type piston cylinder device with a piston diameter of 14 mm. The assemblies used were composed of an outer NaCl sleeve and inner Pyrex and BN sleeves and calibrated against quartz-coesite (1000°C), jadeite-albite-quartz (600°C), and the melting points of

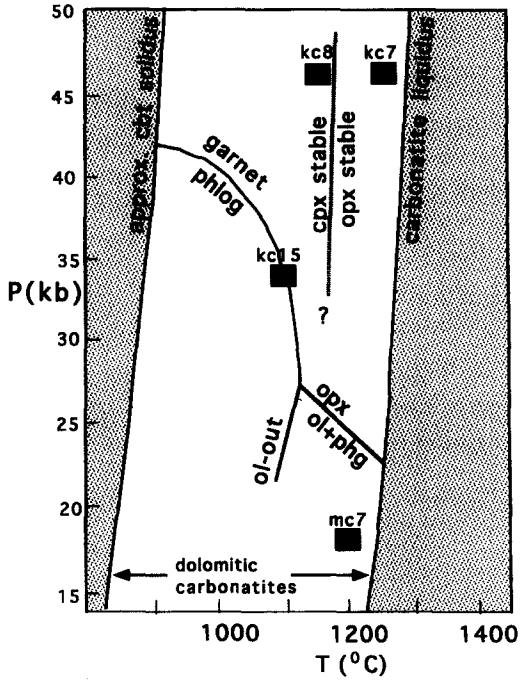

FIG. 1. Phase relations in the carbonate (dolomitic)-dominated bulk systems (Table 1) with the experiments used for partition determinations labelled (simplified after Figs. 1 and 3, Sweeney, 1994).

LiCl and CsCl. Pressure is considered accurate to ±1 kb and temperature to ±10°C for the type-S thermocouples used. No correction for pressure on thermocouple emf was applied.

The experiments at 34 kb (kc15), 40 kb (rg9), and 46 kb (ma1, kc7, kc8) were carried out in a Walker-type (Walker et al., 1990) multianvil device using 12 mm MgO TEL octahedra calibrated at higher temperature in the range 30–100 kb (P. Ulmer and R. J. Sweeney, unpubl. data). Tapered graphite furnaces were used to minimise the temperature gradient. Temperature was monitored using two thermocouples (type S) inserted laterally from the fins. Pressure is considered accurate to ±2 kb and temperature to ±20°C.

The phase relations for the silicate phases crystallizing from the two carbonate bulk compositions and the approximate locations of the solidus and liquidus was similar (Sweeney, 1994) and are shown in Fig. 1. The relative abundances of crystallizing phases in the carbonatite experiments are given in Table 2. In all instances the carbonate melt quenched to a dolomitic spinifex texture. The lower pressure (15–35 kb) phase relations of the MARID bulk composition is given in Sweeney et al. (1993). At these lower pressures, however, garnet was never stabilized on the liquidus. The single experiment at 46 kb and 1400°C (ma1) stabilized the assemblage garnet + orthopyroxene + olivine + clinopyroxene in a capsule containing ca. 80 vol% quenched melt about 100°C above the solidus. Only the garnets in ma1 were sufficiently large for PIXE determinations. The experi-

Table 2. Summary of experimental run conditions and analysed phases (Fig. 1). Bulk composition for each experiment is numbered in parenthesis corresponding to the compositions in Table 1.

Experiment	bulk	P (kb)	T (C)	apparatus	run time (min)	capsule	crystallizing phases in order of abundance	analysed (PIXE) phases (number of determinations)
Silicate bulk systems								
rg9	(2).	42	1200	MA	65	Pt	cpx>ga	cpx (4)
ma1	(1).	46	1400	MA	30	Pt	ga>ol>opx>cpx	ga (1)
Carbonate bulk systems								
kc7	(4).	46	1250	MA	36	Ag50Pd50	dol>ga>opx	opx (4), dol (1)
kc8	(4).	46	1150	MA	60	Ag50Pd50	dol>ga>cpx	cpx (2); ga (2)
kc15	(4).	34	1100	MA	35	Ag50Pd50	ga>dol>cpx>phg>mags	ga (2)
mc7	(3).	18	1200	PC	130	Ag50Pd50	ol>phg	ol (2); phg (3)

(abbreviations: PC=piston cylinder, MA=multi-anvil, ol=olivine, cpx=clinopyroxene, ga=garnet, phg=phlogopite, dol=dolomite, mags=magnesite).

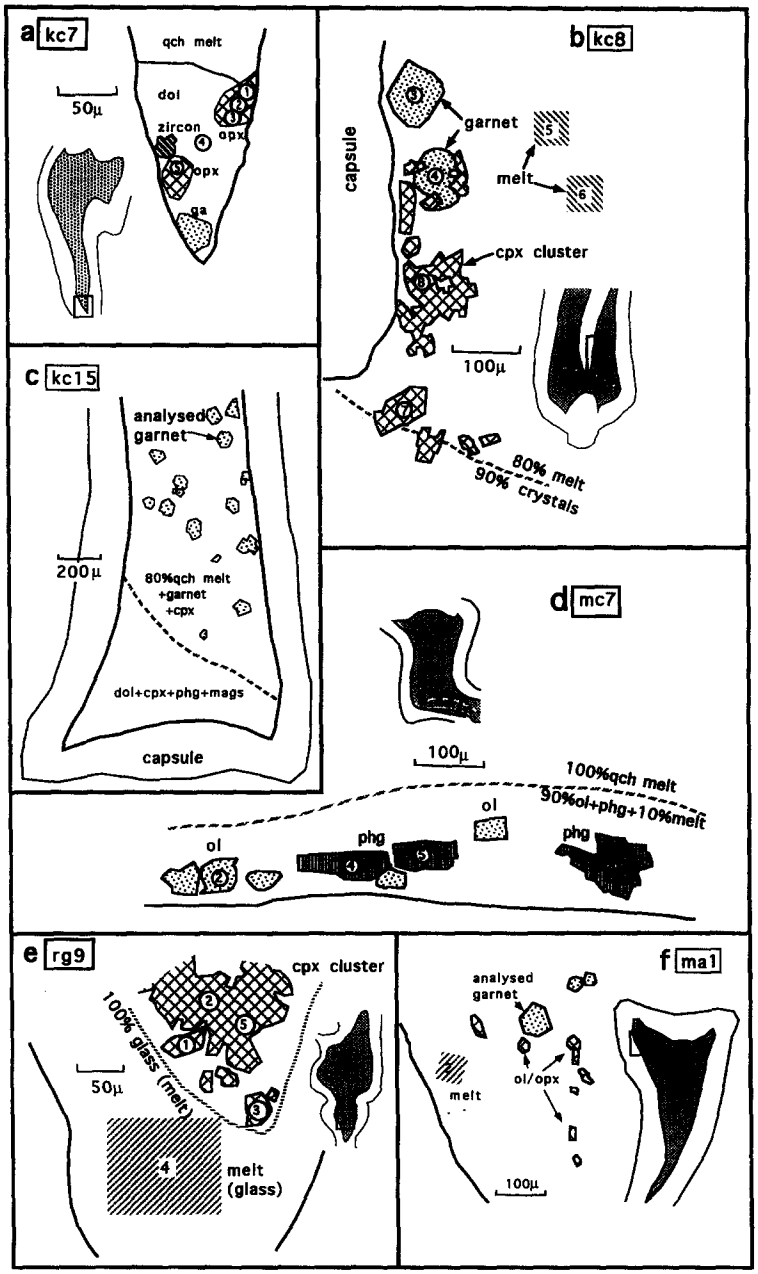

FIG. 2. Sketches of experimental run products analysed by PIXE. Boxes on insets indicate the local position of the illustrated region, except for kc15 where the whole capsule is shown. Crystallizing phases are euhedral to subhedral in shape. In the case of the carbonatite runs (a–d) the melt quenched to predominantly dolomitic quench crystals. The melt in the basalt experiment (e) quenched to a glass, and the melt in ma1 (f, MARID bulk composition) quenched to a glass with phlogopite quench crystals. The analyses numbers correspond to the data given in Tables 4 and 5. The spot sizes illustrated correspond approximately to the PIXE beam area. Garnets are stippled and melt areas analysed in the illustrated portions of capsules are shaded.

ment using the quartz tholeiite bulk composition (rg9) contained small garnets with larger clinopyroxenes in equilibrium with a melt quenched to a glass. The location and distribution of the analysed minerals in the experiments is given in Fig. 2. In all instances the analysed phases are in contact with quenched melt. While there is no independent method to assess equilibrium in these runs, the proportion of melt in all runs is >60 vol%, and equilibration is likely to be rapid.

3. ANALYTICAL METHODS

Run products were analysed using electron-beam microanalysis (EPMA) with a Cameca SX50 wavelength dispersive electron microprobe (Na, K) and proton-beam microanalysis using proton-induced X-ray emission (PIXE). The elements Si, Ti, Cr, Al, Fe, Mg, Ni, Ca, Na, and K were analysed by EPMA techniques (Zurich). An accelerating potential of 15 kV and beam current of 20 nA was used and typical precisions were 3% relative with lower limits of detection in the range 0.05–0.08 wt% for the counting times used. The beam size varied from 1–3 μm (for silicate minerals) to 10–50 μm for quenched melts.

The elements Fe, Ti, Cr, Ni, Nb, Zr, Ta, Y, Ce, Nd, Lu, Sr, Rb, Ba, Ag, Pd, Zn, and V were analysed by proton-induced X-ray emission (PIXE) at the National Accelerator Centre (NAC) in South Africa. The PIXE probe is based on a 6 MV single-ended Van de Graaff

Table 3. Analytical precision of PIXE methods.

	TESTD known	TESTD CSIRO	TESTD NAC conc.	TESTD count stats	TESTD lld	garnet conc.	garnet count stats	garnet lld
	1	2	3	4	5	6	7	8
%								
FeO	6.12	tied	6.34	0.13	0.003	6.80	0.14	0.003
TiO_2						1.26	0.10	0.10
ppm								
Nb	1281	1311	1266	32	24	170	19	17
Zr	1536	1585	1520	33	22	2199	41	17
Ta	883	902	929	38	38	197	11	34
Y	931	928	906	23	19	2336	48	16
Lu	607	490	655	32	43	2679	72	40
Ba	1752	1622	1664	323	277	<290		290
Sr	1059	1096	1045	27	17	668	16	13
Rb						<11		11
Ag						590	63	41
Pd						414	36	32

1. Known values of TESTD synthetic glass (Sweeney et al., 1994).
2. Analysis of TESTD by PIXE at CSIRO (Sweeney et al., 1994).
3. Analysis of TESTD by PIXE at NAC (this study) for an accumulated charge of 0.3 micro-Coulombs.
4. Counting statistics for column 3 calculated for 1 standard deviation.
5. Lower limit of detection for column 3 calculated at the 99% confidence interval.
6. Garnet analysis from run kc15 for an accumulated charge of 0.4 micro-Coulombs.
7. Counting statistics for column 6 calculated for 1 standard deviation.
8. Lower limit of detection for column 6 calculated at the 99% confidence interval.

accelerator and uses Oxford Microprobe triplet lenses for beam focusing (Tapper et al., 1993). In this application a 3 MeV proton beam was used, collimated using two sets of slits 5 m apart and focused by a triple set of quadruple lenses. The relatively long beam path length and high ion flux, enabled beam dimensions of ca. 0.5 μm horizontally and ca. 2 μm vertically to be obtained (Tapper et al., 1993). For quantitative determinations in this study, the beam was focused to between 10–15 μm for silicates and rastered over areas 40–200 μm in diameter for the quenched carbonate/silicate matrix (see Fig. 2). The X-rays were detected using a Si (Li) detector positioned at 135° with respect to the incident beam. Measurements were carried out with an 80.4 μm thick Al filter positioned before the detector which attenuated the count rate (principally the major element Fe) to acceptable levels to reduce peak pile-up effects. The charge accumulated varied from 0.3–1.5 μC, depending on desired precisions and lower limits of detection. The energy dispersive spectra were analysed using GeoPIXE software (Ryan et al., 1990a,b). The PIXE setup was calibrated earlier (Van Achterbergh et al., 1993) and accuracy was confirmed against the trace element standard BCR-1 and a secondary standard (TESTD in Table 3) containing the trace elements of interest to this study. Reproducibility was found to be better than ±5% relative for duplicate analyses of the secondary standard and compared well to values obtained at CSIRO (Table 3). Counting precisions and limits of detection are given for a standard glass analysis and for a typical garnet analysis in Table 3.

The focusing of the beam to less than 15 μm diameter for phases eliminated the possibility of lateral overlap from adjacent minerals or melt but not the possibility of overlap from underneath the grains. Two factors influence the degree of penetration of any X-rays from a matrix underlying a mineral, the wavelength of the analyte radiation (for example, Sr Kα with an X-ray energy of 14.1 keV will penetrate more easily than Ta Lα with an X-ray energy of 8.1 keV) and the degree to which the abundance of an element in the matrix exceeds that of the mineral. The maximum penetration depth of the beam was assessed by considering a case where both the factors above were maximised. This is the case for a garnet grain (from kc15, Table 3, Fig. 2c) which has 668 ± 34 ppm Sr, embedded in a carbonatite quenched melt containing 10770 ppm Sr. The Sr Kα scan may be compared with the Ta Lα scan produced by rastering a beam estimated to be < 5 μm in diameter over the grain for 8 h (Fig. 3). The Ta Lα scan shows an even distribution of Ta in the garnet and very little penetration (<10 μm) of Ta Lα radiation from the underlying matrix which has a much higher Ta content (1406 ppm) (Fig. 3a). In contrast, the Sr Kα scan shows an apparent zonation in the garnet (Fig. 3b). However, Ta and all other elements scanned (Fe, Cr, Y, Zr, Nb, Pd, Ag) show even distributions, so this zoning is due to the penetration of the Sr Kα radiation from the Sr-rich underlying matrix. If a hemispherical grain shape is assumed, then simple geometry suggests a maximum penetration depth of 28 μm for Sr Kα. The high abundance of Sr in the matrix (percent level) and the relatively high energy of Sr Kα radiation makes this penetration depth a likely maximum. We estimate the effective depth of analysis in most instances (e.g., 1000 ppm in the matrix and lower energy radiation) is 10–15 μm. Thus, in this study all grains analysed were constrained to be >15 μm in radius (Fig. 2) to minimize any potential overlap problems. Analysed grains were examined optically to avoid inclusions exposed on the surface, but it was difficult to avoid sampling unseen subsurface inclusions with the proton beam and this may be a source of error in the data.

To test mineral and melt homogeneity, the electron probe was calibrated for selected trace elements and garnets from #run ma1 and melts from #run mc7 were analysed repeatedly (Table 4). The quench carbonatite melt was very homogeneous with 1 standard deviation statistical errors < 20% relative (within analytical uncertainty). The PIXE rastered images (Fig. 3) suggest that the melt is generally homogeneous (Ta 700–1000 ppm and Sr 8400–12000 ppm) within the resolution of the finely focused (ca. 5 μm) PIXE beam. EPMA data obtained for trace element abundances in the garnets analysed are 15–20% relative (1 standard deviation statistical error) for the dataset obtained (Table 4). This is similar to the expected analytical uncertainty (±150 ppm) for this concentration for the analytical parameters used (e.g., Sweeney et al., 1994). Although Ta showed an even distribution in the garnet scanned by PIXE (Fig. 3a), occasional high Ta spots in the garnet scanned using a finely focused proton beam suggest that trace elements in garnet may form local clusters. The use of a defocused proton beam (10–15 μm) for analytical determinations, however, will not resolve this local clustering.

The data in Table 4 may also be used to compare the PIXE and EPMA techniques. The EPMA data from carbonate melts agrees with the PIXE data (compare Tables 4 and 6). A garnet from experiment ma1 was chosen for EPMA determinations as the D's obtained using PIXE were significantly different from published values (see Fig. 4b, discussed below). Nb and Ta determined by EPMA have much lower abundances relative to PIXE and would give D's more consistent with published data. The most likely explanation is matrix overlap elevating abundances in the ma1 garnet in the case of PIXE.

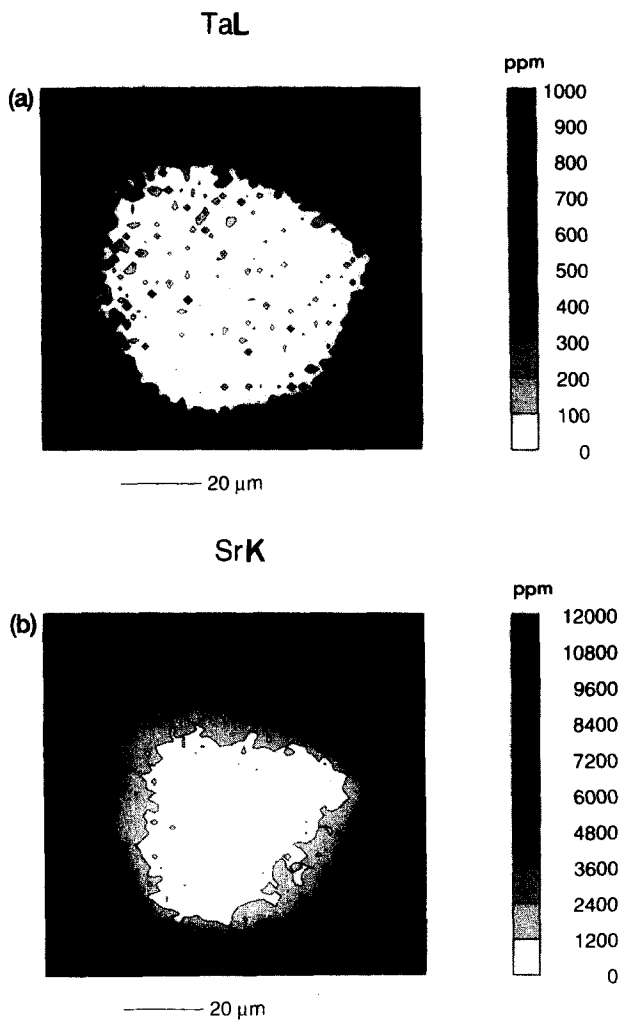

FIG. 3. X-ray scan for Ta Lα and Sr Kα in a garnet (kc15, Tables 3, 5) encapsulated by quenched dolomitic carbonatite melt. The edge of the garnet grain at the surface is clearly delineated within 5μm (the resolution of the scan) in the Ta Lα scan (a) which corresponds approximately with the 7200–8400 ppm contours on the Sr Kα scan (b).

4. RESULTS

Partition coefficients are calculated from the data in Tables 5–7 and given in Table 8. Where multiple analyses were carried out, the PIXE mineral data used to calculate the D's were the data with the minimum incompatible element content (asterixed values). In the case of the carbonatite D's, the analysed Sr content of minerals was used to assess the likelihood of significant contributions from any underlying carbonatite matrix. Strontium is particularly sensitive in this regard (see above discussion), primarily because of the high Sr content of all quenched carbonate matrixes (9300–10800 ppm, Table 7) relative to minerals. For example, in experiment mc7, carbonate matrix contributions will be minimized in olivine 1 (Sr 183 ppm) compared with olivine 2 (Sr 977 ppm).

4.1. Clinopyroxene

There is no significant difference in the D's for clinopyroxene when equilibrated with a carbonatite or silicate melt (Fig. 4a). In the case of the silicate measurements (experiment rg9) the clinopyroxene analysis used was obtained from a cluster of grains (Fig. 2e) and the possibility exists that some interstitial melt may have been included in this determination. The carbonatite measurement used, however, was obtained on a single large clinopyroxene grain in experiment kc8 (analysis 7 in Fig. 2b), where the possibility of matrix overlap is less likely. While we cannot categorically exclude matrix overlap in the case of the clinopyroxene determinations in this study, the D's obtained are mostly consistent with published data (Table 9) with only some D's obtained in this study elevated compared to the total range in published values (Fig. 4a).

There are no systematic differences in D^{cpx} with major element content of the clinopyroxene which varies substantially from the eclogitic bulk composition to those crystallized from the carbonatite melts: the latter are more magnesian, less aluminous, and less sodic, and more representative of those found in peridotites. The similarity in D^{cpx} between silicate

Table 4. EPMA determinations on selected minerals.

	garnet										orthopyroxene	
run#	ma1										kc7	
	within grain				separate grains			av	1sd		separate grains	
%												
FeO	3.80	4.99	3.77	4.20	3.68	4.01	3.58	4.00	0.48		5.07	5.19
ppm												
Ti	7010	9710	6890	9140	6910	8220	7080	7851	1181		480	530
Nb	<150	<150	<150	<150	<150	<150	<150				<150	<150
Zr	890	1420	920	1100	860	1100	860	1021	204		160	240
Ta	310	360	220	210	290	210	260	266	57		<150	<150
Y	3730	5030	3810	4080	3400	4690	3360	4014	635		<150	<150

	melts									
run#	mc7									
%									av	1sd
FeO	5.69	5.56	4.81	4.85	4.71	5.23	5.29	5.44	5.20	0.37
ppm										
Ti	6600	5900	5300	5200	5300	5800	5900	5500	5688	464
Zr	920	890	890	940	780	820	890	940	884	57
Nb	1100	1080	1010	920	960	1070	1000	1160	1038	79
Ta	410	230	310	340	320	360	400	250	328	65
Y	310	350	310	340	300	320	280	300	314	23
Nd	580	550	500	560	530	500	480	570	534	37

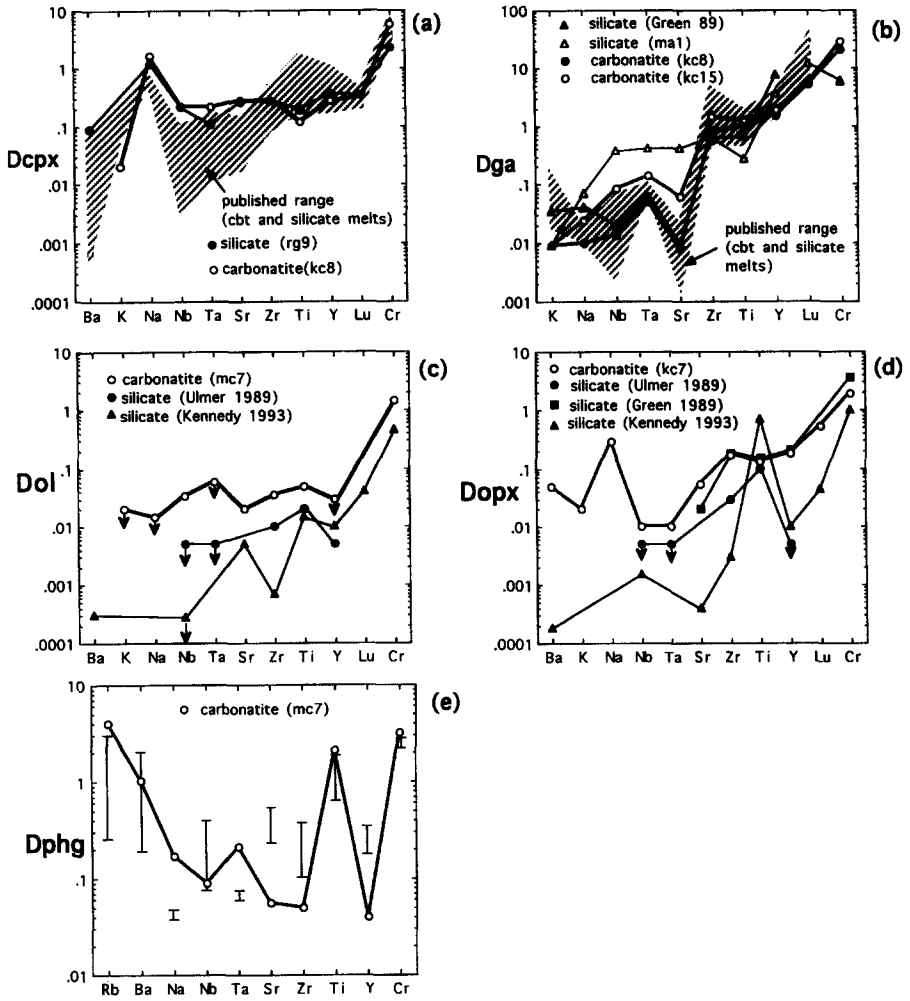

FIG. 4. Individual mineral partition coefficients (D = concentration in mineral/concentration in melt) for silicate- and -carbonatitic melts obtained in this study (Table 8). When detection limits in the mineral are reached, the maximum D is plotted (indicated by arrows). The shaded fields in (a) and (b) are the ranges in published data for silicate- and carbonatite-melts (see Table 9). Individual values for garnet-silicate melt (b) are from Green et al. (1989) measured in a tholeiitic bulk composition at 12 kb. The $D^{ol\text{-}silmelt}$ and $D^{opx\text{-}silmelt}$ coefficients are from Ulmer (1989) measured in a picritic bulk composition at 28 kb, Green et al. (1989) at 25 kb and Kennedy et al. (1993) at 1 atmosphere. The bars indicate the range in data for $D^{phg\text{-}silmelt}$ from data in Adam et al. (unpubl. data in Green, 1994) at 20 kb in a basanite (Rb, Ba, Nb, Ta, Sr, Zr, Ti, Y, Lu), Dalpe and Baker (1993) at 15 kb in a nephelinite (Rb, Nb, Sr, Zr, Ti, Y), Guo and Green (1990) at 10–30 kb in a lamproite (Ba, Ti), and include Ti, Na, and Cr from Sweeney et al. (1993) at 30 kb in an ultramafic potassic xenolith (MARID AJE137).

and carbonate liquids, shows that inter element fractionations between carbonate and silicate liquids will not be significant (Fig. 4a).

Determination of D^{cpx} for selected elements with silicate melt at 30 kb enabled Blundy and Wood (1994) to determine elastic moduli for the substitution of +1, +2, and +3 cations into the M2 site in diopside and the optimum ionic radius of this site. Blundy and Wood (1994) derived an expression describing D_i (partition coefficient of element i) as a function of D_0 (a strain-free partition coefficient and is equal to D_{Ca} for the M2 site in diopside), elastic modulus, and radius of the site and ionic radius of the element of interest, for a particular P, T and X. For example, the ionic radius of Sr under eightfold coordination is 1.25A (Shannon, 1976), and the theoretical D for Sr in clinopyroxene may be calculated for the bulk systems in this study using Eqn. 3 of Blundy and Wood (1994). This calculation gives D^{cpx} for Sr of 0.16 for rg9 (silicate bulk system) and 0.05 for kc8 (carbonate-dominated bulk system) using D_{Ca} of 2.27 and 0.79, respectively (Tables 5, 7). The value calculated for the silicate bulk system is quite similar to the experimental value obtained here (0.26), but the value for carbonate bulk system is different (0.05) compared with this study (0.26), but similar to those obtained in other studies (0.03–0.08, Table 9).

4.2. Garnet

$D^{ga\text{-}cbtmelt}$ were measured in two experiments (kc8, kc15) in this study and these determinations are mostly within the range of published values for carbonatite and silicate melts (Fig. 4b, Table 9). The measurements of $D^{ga\text{-}silmelt}$ for Nb, Ta, and Sr obtained in this study (experiment ma1), however, are

Table 5. Major element compositions of minerals determined by EPMA. Elements not determined are indicated by blanks.

	Silicate bulk system			Carbonate-dominated bulk system														
	cpx	garnet	garnet	olivine	olivine	opx	cpx	cpx	cpx	garnet	garnet	garnet	garnet	phg	phg	phg	phg	phg
run#	rg9	ma1	ma1	mc7	mc7	kc7	kc8	kc8	kc8	kc8	kc8	kc8	kc15	mc7	mc7	mc7	mc7	mc7
P(kb)	40	46	46	18	18	46	46	46	46	46	46	46	34	18	18	18	18	18
T(C)	1200	1400	1400	1200	1200	1250	1150	1150	1150	1150	1150	1150	1100	1200	1200	1200	1200	1200
		core	rim*															
%																		
SiO2	54.55	42.63	43.39	41.05	41.14	55.97	54.66	53.92	54.74	41.13	41.29	41.33	41.24	38.91	38.27	39.20	39.77	40.50
TiO2	0.49	1.61	1.11	<0.05	<0.05	0.09	0.09	0.13	0.06	0.49	0.72	0.68	0.86	1.99	1.95	2.02	1.97	1.96
Cr2O3	0.11	0.83	0.42	<0.10	<0.10	0.55	1.36	1.43	0.96	2.89	3.90	3.71	4.50	0.69	0.67	0.69	0.78	0.30
Al2O3	10.25	21.90	22.72	<0.05	<0.05	2.88	2.91	3.13	1.84	19.76	18.61	18.99	18.14	16.92	17.12	16.29	17.46	16.72
FeO	3.41	4.33	3.55	7.57	7.41	5.20	2.94	3.02	2.94	7.41	7.19	7.26	7.48	4.70	4.68	4.50	4.50	4.82
MgO	11.29	21.50	22.26	49.96	51.19	32.94	17.88	16.94	18.76	18.71	18.36	18.51	17.95	21.04	21.15	21.92	21.40	22.36
NiO	<0.10	<0.10	<0.10	0.27	0.20	<0.10	<0.10	<0.10	<0.10	<0.10	<0.10	<0.10	<0.10	<0.10	<0.10	<0.10	<0.10	<0.10
CaO	15.30	7.16	5.89	0.11	0.11	2.35	19.25	19.92	19.69	8.95	9.82	9.72	9.93	<0.05	<0.05	<0.05	<0.05	<0.05
Na2O	4.21	0.08	0.11	0.38	0.12	0.08	1.22	1.39	0.93	0.05	0.07	0.06	0.05	0.60	0.50	0.50	0.55	0.71
K2O	<0.05	0.10	0.14	<0.05	<0.05	0.06	0.10	0.12	0.09	0.06	0.07	0.05	0.05	9.04	8.77	8.75	9.03	8.76
sum	99.61	100.14	99.59	99.34	100.17	100.12	100.41	100.00	100.01	99.45	100.03	100.31	100.20	93.89	93.11	93.87	95.46	96.13
cations for	6ox	12ox	12ox	4ox	4ox	6ox	6ox	6ox	6ox	12ox	12ox	12ox	12ox	12ox	12ox	12ox	12ox	12ox
Si	1.945	2.993	3.032	1.003	0.995	1.931	1.961	1.951	1.973	2.989	2.999	2.991	3.001	2.791	2.766	2.806	2.798	2.824
Ti	0.013	0.085	0.058	0.000	0.000	0.002	0.002	0.004	0.002	0.027	0.039	0.037	0.047	0.107	0.106	0.109	0.104	0.103
Cr	0.003	0.046	0.023	0.000	0.000	0.015	0.039	0.041	0.027	0.166	0.224	0.212	0.259	0.039	0.038	0.039	0.044	0.017
Al	0.431	1.812	1.871	0.000	0.000	0.117	0.123	0.133	0.078	1.692	1.593	1.620	1.556	1.431	1.459	1.374	1.448	1.374
Fe2	0.102	0.254	0.208	0.155	0.150	0.150	0.088	0.091	0.089	0.450	0.437	0.439	0.455	0.282	0.283	0.269	0.265	0.281
Mg	0.600	2.250	2.318	1.819	1.844	1.694	0.956	0.914	1.008	2.026	1.987	1.997	1.947	2.250	2.279	2.339	2.244	2.324
Ni	0.000	0.000	0.000	0.005	0.004	0.000	0.000	0.000	0.000	0.000	0.000	0.000	0.000	0.000	0.000	0.000	0.000	0.000
Ca	0.584	0.539	0.441	0.003	0.003	0.087	0.740	0.772	0.760	0.696	0.764	0.753	0.774	0.000	0.000	0.000	0.000	0.000
Na	0.291	0.011	0.015	0.018	0.006	0.005	0.085	0.097	0.065	0.008	0.009	0.009	0.007	0.084	0.070	0.069	0.075	0.096
K	0.000	0.009	0.012	0.000	0.000	0.003	0.005	0.006	0.004	0.005	0.006	0.005	0.004	0.828	0.809	0.799	0.810	0.779
sum cat	3.969	8.000	7.977	3.003	3.001	4.004	4.000	4.009	4.005	8.059	8.058	8.063	8.049	7.812	7.810	7.803	7.786	7.797
Mg#	85.5	89.8	91.8	92.2	92.5	91.9	91.6	90.9	91.9	81.8	82.0	82.0	81.0	88.9	89.0	89.7	89.4	89.2

*used for partition coefficient calculation

significantly greater than previously published values (Green et al., 1989 shown individually in Fig. 4b). EPMA determinations of Ta and Nb in ma1 garnets indicated much lower concentrations than the PIXE data which was used to calculate the partition coefficients (Tables 4, 6), however, and we suggest that the PIXE data for ma1 in this study has been affected by overlap with the matrix (D's bracketed in Table 8). Comparing values obtained for $D^{\text{ga-cbtmelt}}$ with literature data for $D^{\text{ga-silmelt}}$, shows no significant differences, with the possible exception of D_{Zr} which is greater for garnet in carbonatite melts (Table 9). Therefore, garnet could not cause any interelement fractionations for the elements determined between silicate and carbonatite melts with the possible exception of ratios involving Zr.

4.3. Olivine and Orthopyroxene

The D's obtained for orthopyroxene and olivine in this study used mineral data on large grains (experiments kc7 and mc7 in Fig. 2) where possibility of matrix overlap is remote. PIXE data obtained for orthopyroxene 1, 2, and 3 in experiment kc7 (Fig. 2a) is also consistent with EPMA determinations (compare Tables 4 and 6).

$D^{\text{ol-cbtmelt}}$ for the elements measured are consistently greater than for silicate melts (Fig. 4c; Ulmer, 1989; Kennedy et al., 1993). Significantly, though, the interelement ratios will not be changed in the melt by equilibration of a different melt-type (carbonatite or silicate) with olivine. D^{opx} for carbonatite melts are similar or greater than D^{opx} for silicate melts, al-

Table 6. Compositions of minerals determined by PIXE. Elements not determined are indicated by blanks. Numbers correspond to data points on Fig. 1.

	Silicate bulk system				Carbonate-dominated bulk system															
	eclogitic				peridotitic	peridotitic														
	cpx				garnet	olivine	orthopyroxene					dolomite	clinopyroxene		garnet		garnet		phlogopite	
run#	rg9				ma1	mc7	kc7					kc7	kc8		kc8		kc15		mc7	
P(kb)	40				46	18	46					46	46		46		34		18	
T(C)	1200				1400	1200	1250					1250	1150		1150		1100		1200	
	1	2	3	5*	*	1*	2	1*	2*	3*	5	4	7*	8	3	4*	core*	rim	4*	5	8
%																					
FeO	4.02	3.17	3.57	3.41	3.62	7.41	7.19	3.64	3.81	3.74	2.07	1.87	3.32	3.35	6.90	6.85	6.80	7.01	6.34	5.90	6.56
ppm																					
Ti	10270	4805	9517	4154	10110	<609	<600	1022	902	635	<85	<85	1963	1839	6606	4967	7530	7574	4652	3861	5229
Cr	1115	1645	1254	1854	4858	1509	1827	3862	4430	3875	721	454	6877	5862	25890	25070	29700	30490	3446	3251	2919
Ni	<18	<14	<16	<13	721	1506	1422	19.3	39	31	17	<7	<14	<16	<21	<21	<17	<18	1103	1015	1060
Nb	1376	715	1426	403	1084	36	107	18.5	<9	<8	<25	<8	400	573	66	25	170	549	96	106	144
Zr	1248	680	1294	444	1578	34	114	377	237	151	3520	9.5	586	661	1768	1672	2199	2083	51	56	111
Ta	1634	798	1658	467	1629	<25	78	16	<12	<13	19	<13	278	369	163	64	197	385	88	97	74
Y	664	386	609	313	3741	<9	26	290	192	130	95	123	318	417	1935	1783	2336	2074	<13	29	25
Ce	3231	2370	2086	817	1012			<270	<222	<520	<270	<170	1323	2559	<642	<578	582	1898	<463	<714	353
Nd	<1500	<1500	<1500	<1135	<882			<680	<493	<950	<570	<540	<1390	<1450	<1350	<1826	<884	<1026	<1024	<1373	<618
Lu	287	215	297	163	3777	<33	<34	312	205	141	93	79	145	138	2285	2264	2679	2460	39	<30	<17
Sr	2038	1172	2148	752	762	183	977	653	378	464	1418	1847	2575	3637	73	81	668	2679	527	703	1019
Ba	3157	1473	2865	<292	2119			<170	<150	<170	<180	<390	1278	3626	<353	<254	<289	1389	2131	2200	1579
Pb	<15	<12	<16	<9	<11	<8	40	<7	<6	<6	12	<7	<12	<22	<12	<13	<11	<15	1351	1458	932
Ag	69	<40	66	<33	<30	748	942	1051	866	816	3181	980	2421	2899	449	365	590	1471	701	1047	1261
Pd	<31	<33	<30	<25	<24	729	853	1065	927	833	3292	1089	673	649	352	251	414	485	683	969	1221
Zn	<13	<11	<13	<9	<15	30.6	40	26	25	22	12	8.8			<13	<12	<13	<13	19	22	29

* used to calculate D's in Table 8

Table 7. Melt compositions. Major elements are determined by EPMA and are averages of multiple determinations. Elements not determined are indicated by blanks

	Silicate bulk system		Carbonate-dominated bulk system				
	eclogitic	peridotitic	peridotitic				
#run	rg9	ma1	mc7	kc15	kc7	kc8	kc8
P(kb)	40	46	18	34	46	46	46
T(C)	1200	1400	1200	1100	1250	1150	1150
EPMA							
%							
SiO2	54.50	44.56	10.73	8.16	7.21	6.50	
TiO2	2.46	4.15	0.95	0.69	0.88	0.76	
Cr2O3	<0.08	<0.08	<0.08	0.10	0.06	0.11	
Al2O3	12.17	9.04	2.60	1.56	1.24	1.11	
FeO	3.31	3.28	5.20	4.07	4.42	4.09	
MgO	2.97	12.14	15.26	13.93	15.46	13.93	
NiO	<0.05	0.05	<0.05	<0.05	<0.05	<0.05	
CaO	6.74	4.96	21.35	21.91	25.65	25.00	
Na2O	3.54	1.13	3.40	2.10	0.28	0.71	
K2O	0.00	11.29	2.93	5.35	3.20	5.76	
Total	85.78	98.27	63.22	57.92	58.65	58.06	
Mg#	61.5	86.8	84.0	85.9	86.2	85.9	
PIXE							
%FeO	3.89	3.45	6.59	5.59	5.18	5.03	
ppm						5*	6*
Ti	17630	24590	7348	5599	6431	8139	6864
Cr	795	807	1065	1035	2111	1173	1215
Ni	<14	528	79	<22	<22	<20	<22
Nb	1826	2919	1069	1982	1809	1718	1949
Zr	1617	2525	932	1550	1482	2091	1949
Ta	4203	4022	423	1406	1455	1125	1362
Y	873	1065	283	1221	1117	1125	1203
Ce	4378	2447	4139	5064	4519	5663	6624
Nd	<1161	<939	837	<1592	<1320	<1423	<1800
Lu	466	316	69	494	423	454	412
Sr	2908	1921	9331	10770	9409	9205	10260
Ba	3309	5454	2047	5027	3388	4129	4724
Pb		<12	342	<20	<22	<21	<22
Ag			1979	3102	3488	4273	4916
Pd			320	539	474	337	383
Zn		52	37	33	31	23	30

* see Fig. 2, average value used to calcuate D's

though considerable variability in the published values for silicate melts is observed (Fig. 4d) and thus, it is difficult to assess what interelement ratios may be fractionated differently between melt types. Generally, the observation that $D^{cbt} > D^{silmelt}$ for olivine and orthopyroxene must be a function of the different bulk compositions (silicate- and carbonate-dominated) and this implies that residual olivine and orthopyroxene would be more efficiently depleted in Nb, Ta, Sr, Zr, Ti, and Y by equilibration with a small degree silicate melt than a carbonatitic melt.

4.4. Phlogopite

The available high pressure data for silicate D^{phg}'s are shown with the carbonatite D^{phg}'s determined here for phlogopite (Fig. 4e). Differences in D^{phg} between silicate and carbonatitic melts is observed for Na, Ta, Sr, Zr, and Y (Fig. 4e). However, in the absence of a larger dataset it would be premature to attach any significance to these differences.

5. SYSTEMATICS OF PARTITION COEFFICIENTS

A way of assessing the internal consistency of partition coefficient data is to plot the log D vs. ionic radius of the element ("Onuma"-type diagrams) which should describe parabolas with maxima corresponding to the lattice site where substitution occurs (Onuma et al., 1968; Blundy and Wood, 1994). Here, we consider the first order effects of ionic radius on D's only, and acknowledge that other considerations such as charge balance constraints (requiring coupled substitutions) are important in quantitative models attempting to describe lattice substitutions. Nickel is excluded from this discussion because of appreciable crystal field effects (Blundy and Wood, 1994). The D-data obtained in this study (non-stoichiometric components of minerals only) for orthopyroxene, garnet, clinopyroxene, and phlogopite partitioning with carbonatite melt is plotted in Fig. 5.

In the case of orthopyroxene and garnet, the expected parabolic shape of the data is obvious (Fig. 5a,b), with maxima corresponding to the ionic radii of the stoichiometric cations for which the elements most likely substitute. In orthopyroxene, substituting cations are most likely Mg and Fe in orthopyroxene (linking strongly bonded SiO_4 tetrahedra), and in garnet these are most likely Mg, Fe, and Ca linking the Si-Al-O network (Deer et al., 1966). In the case of clinopyroxene, the relationship between ionic radius and D is less clear, but still parabolic with a maximum corresponding to the ionic radii of the main stoichiometric cations in the M1 and M2 positions (Mg, Fe, Ca, Fig. 5c). In an experimental study at 30 kb, Blundy and Wood (1994) obtained the optimal radius

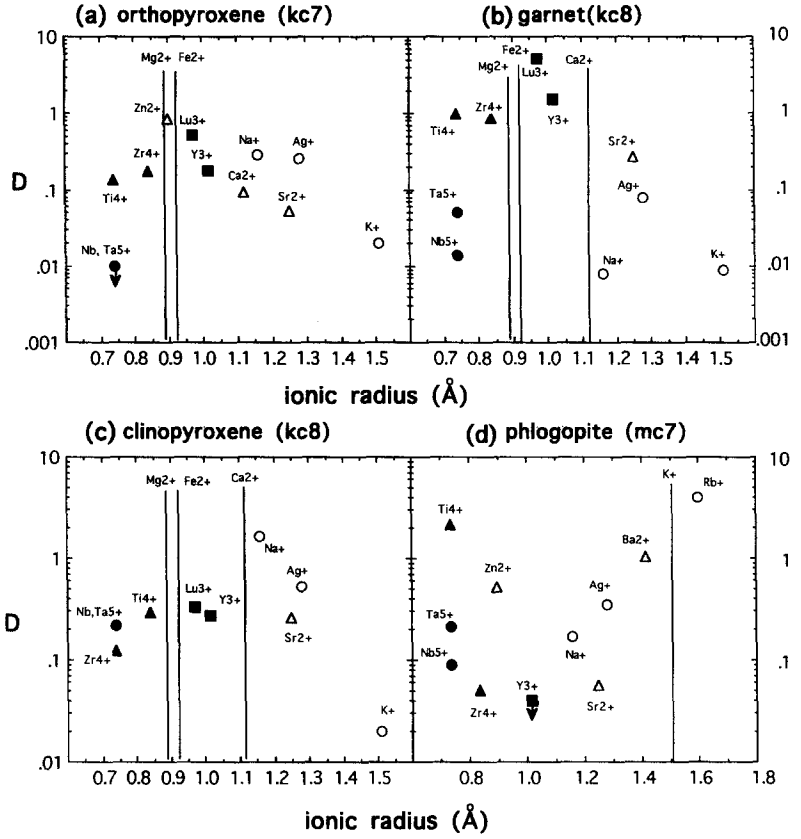

FIG. 5. Carbonatite-mineral D's plotted vs. ionic radii (in angstroms) for octahedral coordination (Shannon, 1976) for nonstoichiometric components (trace and minor elements) in minerals. (a) Orthopyroxene carbonatite melt D's for experiment kc7 (Table 8). (b) Garnet D's are measured values for experiment kc8 for carbonate melts (Table 8). (c) Clinopyroxene D's are those used for modeling (Table 10) and representative of the range in the literature for silicate and carbonate D's (Fig. 4a). (d) Phlogopite D's are measured values for carbonate melts from experiment mc7 (Table 8). Also plotted are the ionic radii of Ca^{2+}, Mg^{2+}, Fe^{2+}, and K^+ under eightfold coordination (discussed in text). Vectored values are maxima (see Table 8).

of the substituting site in clinopyroxene which they assumed to be the M2 (Ca) site. Their value of 1.05 Å is quite similar to the ionic radius of Ca^{2+} (1.12 Å, Shannon, 1976) and is a median value between the ionic radii of Mg^{2+}, Fe^{2+}, and Ca^{2+} (Fig. 5c). Thus, the data for clinopyroxene in this study are consistent with maximum site substitution for ions similar in radius to both M1 and M2 cations (Mg^{2+}, Fe^{2+}, and Ca^{2+}) in clinopyroxene. The plot of D^{phg} for carbonatite melts vs. ionic radii shows a significant departure from the parabolic shapes described by the other minerals measured (Fig. 5d). There are two maxima at large and small ionic sizes, and a minimum at Y^{3+}. It is suggested that this reflects the strongly bimodal site distribution in phlogopite represented by K (between planes) and the much more closely coordinated octahedral cations (Mg, Al, or Fe, within planes) (Deer et al., 1966). The larger cations with similar ionic charge and radius would substitute for K (i.e., Rb, Ba, Ag, Na, Sr), while the remainder would substitute within the planes (for Mg, Al, or Fe).

6. DISCUSSION

6.1. A Model

Two factors govern the effectiveness of mantle minerals to fractionate interelement ratios when residual to any melt: mineral abundance and relative differences in the D's of two elements comprising a ratio. Using numerical models, we consider the manner in which trace element ratios may be fractionated in a residual peridotite affected by the passage of a silicate or carbonatite metasomatic melt.

A two-stage model is examined. The effect on the chemistry of a silicate melt extracted later from a peridotite previously equilibrated with a silicate or carbonate melt is considered. We have explicitly excluded amphibole in these models as it may be a residual phase in only a restricted P-T range (22–30 kb, Wallace and Green, 1988) and therefore, is probably not volumetrically significant for fractionating trace element ratios in the upper mantle as a whole. To constrain peridotite mineralogy, mineral modes (x_i) for Cratonic- and Oceanic-garnet-bearing peridotites are representative of the variation in the source which may exist in the mantle at pressures > 30 kb (i.e., outside pargasite amphibole stability, Wallace and Green, 1988) and are given in Table 10 (Mathias et al., 1970; Maaløe and Aoki, 1977; Boyd, 1989). This enables the calculation of a bulk partition coefficient ($D = \Sigma\, x_i \cdot D_i$ for j minerals) for the source residue. Mineral-melt D's (D_i) are selected using the available experimental data obtained at high pressure (Fig. 4, Tables 8, 9). Where there are no significant differences between $D^{min\text{-}cbtmelt}$ and

Table 8. Mineral-melt partition coefficients (concentration mineral/concentration in melt)
Where multiple EPMA data is available, averages are used. PIXE data used is indicated in Table 7.

	Silicate bulk system		Carbonate-dominated bulk system					
	eclogitic	peridotitic	peridotitic					
	cpx	garnet	ol	opx	cpx	garnet		phlogopite
run#	rg9	ma1	mc7	kc7	kc8	kc8	kc15	mc7
P(kb)	40	46	18	46	46	46	34	18
T(C)	1200	1400	1200	1250	1150	1150	1100	1200
Kd's								
Ti(EPMA)	0.20	0.27	<0.05	0.13	0.12	0.99	1.2	2.1
Cr	2.3	6.0	1.4	1.9	5.8	21.0	28.7	3.2
Ni	-	1.4	19.1	-			-	14.0
Nb	0.22	[0.37]	0.034	<0.01	0.22	0.014	0.086	0.09
Zr	0.27	[0.62]	0.036	0.17	0.29	0.83	1.42	0.05
Ta	0.11	[0.41]	<0.06	<0.01	0.22	0.051	0.14	0.21
Y	0.36	3.51	<0.03	0.18	0.27	1.53	1.91	<0.04
Ce	0.19	[0.41]	-	<0.05	0.22	-	0.11	-
Lu	0.35	12.0	-	0.52	0.33	5.2	5.4	[0.57]
Sr	0.26	[0.40]	0.020	0.053	0.26	0.008	0.062	0.056
Ba	<0.09	[0.39]	-	<0.05	-	-	-	1.04
Rb	-	-	-	-	-	-	-	4.0
Ag	-	-	0.38	0.26	0.53	0.08	0.19	0.35
Pd	-	-	2.3	2.0	1.9	0.08	0.77	2.1
Zn	-	-	0.83	0.79	-	-	-	0.51
Na(EPMa)	1.19	0.071	<0.015	0.29	1.66	0.008	0.020	0.17
K(EPMA)	-	0.009	<0.02	0.02	0.020	0.009	0.009	3.03

[ ] values are uncertain due to matrix overlap effects (garnet in experiment ma1) or analytical uncertainty (Lu in phlogopite in experiment mc7).

$D^{\text{min-silmelt}}$, then the same values are used for equilibration with the stage 1 metasomatic silicate or carbonatite melts. This is the case for D^{cpx} and D^{ga}, except for D_{Zr} and D_{Cr} in garnet which may be significantly different between melt types (Tables 8, 9).

These bulk partition coefficients are plotted in Fig. 6a, and show the greater retention of Na, Nb, Ta, Sr, Zr, and Cr in a peridotite residue which has equilibrated with a carbonatite melt relative to a silicate melt (after stage 1). The composition of the residue (c_r) after the passage of a metasomatic liquid (c_m) may then be calculated from the definition: $D_{sl} = c_r/c_m$ (concentration in residue/concentration in metasomatic liquid), where D_{sl} is the bulk partition coefficient for stage 1. The concentration in the residue (c_r) then becomes the starting concentration of the second stage melting event (c_0). The enrichment (c_1/c_0) in any second stage melting

Table 9. Published D's obtained at elevated pressures for selected elements.

	Silicate melt (basaltic) - mineral bulk systems													
	orthopyroxene		garnet				clinopyroxene							
	Green89	Ulm89	Green89	Ulm89	John94	Jenn94	Green89	Ulm89	John94	HD93	Jenn94	AG94
Ti(EPMA)	0.23	0.1	0.65	0.28	0.28	1.0	0.43	0.18	0.347	0.384	0.37	0.30
Cr	3.7		5.7				6.6			3.8		
Nb		0.005	0.02	0.07	0.0042	0.03	0.005	0.02	0.004	0.0077	0.004	
Zr	0.18	0.03	0.6	0.32	0.27	0.73	0.1	0.1	0.128	0.123	0.21	
Ta		0.005	0.06	0.04		0.126	0.013	0.02			0.019	
Y	0.18	0.005	7.4	2.11	2.8	7.1	0.9	0.2	0.421	0.467	0.72	
Lu					7.1				0.439	0.433		0.49
Sr	0.02		0.01		0.003	0.006	0.06		0.096	0.128	0.096	
Ba										0.0007		
Na(EPMa)				0.04			1.19	0.6				
K(EPMA)					0.035				0.07			

	Carbonate melt - mineral bulk systems				
	garnet			clinopyroxene	
	Green92	Sw92-27	Sw92-33	Green92	Kle95
Ti(EPMA)		1.7	0.5		1.42
Cr		>23	>23		
Ni					
Nb	0.003	0.012	0.023	0.01	0.1
Zr	0.54	3.98	1.6	0.29	0.48
Ta		0.095	<.07	0.03	0.15
Y	1.4	3.06	2.06	0.22	0.3
Lu	11.6	>30	17.7	0.23	
Sr	0.003	0.0017	0.019	0.03	0.08
Ba	0.003	<.02	0.027	0.006	0.07
Rb		<.004	0.021	0.004	
Na(EPMa)		0.016	0.012		
K(EPMA)		<.15	<.021		

Data from Green et al. (1989) [Green89, 25kb], Ulmer (1989) [28kb], Green et al. (1992) [Green92, 25kb]
Sweeney et al. (1992) [Sw92, 27kb and 33kb], Johnson (1994) [John94, 20kb],
Jenner et al. (1994) [Jenn94, 25kb], Hart and Dunn (1993) [HD93, 30kb],
Adam and Green (1994) [AG94, 20kb], Klemme et al. (1995) [Kle95, 21kb].

Table 10. Model parameters for melting of a metasomatised mantle source. Phlogopite in source modes is assumed and the melting mode chosen gives phlogopite exhaustions at 6.6% melting in cratonic- and 3.3% melting in oceanic-peridotites. D's are consistent with Table 9 and Fig. 4. D_{Na} and D_K in olivine and orthopyroxene, and D_K for phlogopite, are assumed.

Mineral modes	cratonic peridotite (1).	oceanic peridotite (2).	melting mode assumed
oliv	0.620	0.786	0.050
opx	0.290	0.120	0.250
garnet	0.050	0.045	0.250
cpx	0.030	0.044	0.300
phlog	0.010	0.005	0.150

Mineral-melt D	oliv	opx	garnet	cpx	phlog
carbonatite melt					
K	0.010	0.020	0.010	0.080	3.000
Na	0.010	0.290	0.050	1.000	0.170
Nb	0.030	0.010	0.015	0.100	0.090
Ta	0.030	0.010	0.050	0.100	0.210
Sr	0.020	0.050	0.008	0.100	0.060
Zr	0.030	0.170	0.800	0.200	0.060
Ti	0.020	0.130	0.900	0.200	2.100
Y	0.020	0.180	1.500	0.300	0.030
Lu	0.020	0.520	6.000	0.300	0.560
Cr	1.400	1.920	20.000	5.000	3.000
silicate melt					
K	0.005	0.010	0.010	0.080	6.000
Na	0.005	0.010	0.050	1.000	0.040
Nb	0.001	0.002	0.015	0.100	0.200
Ta	0.001	0.002	0.050	0.100	0.070
Sr	0.007	0.010	0.008	0.100	0.300
Zr	0.010	0.030	0.600	0.200	0.300
Ti	0.020	0.200	0.900	0.200	1.000
Y	0.005	0.005	1.500	0.300	0.300
Lu	0.045	0.045	6.000	0.300	0.200
Cr	0.450	2.000	6.000	5.000	3.000

1 Maaloe and Aoki (1977), Mathias et al. (1970), Boyd (1989)
for subcratonic xenoliths from South Africa.
2 Boyd (1989)

event (to generate a basaltic silicate liquid) may be calculated from the equation for equilibrium melting (Gast, 1968; Shaw, 1970), substituting for c_0 using $c_0 = D_{s1} * c_m$ then

$$c_l/c_m = D_{s1}/[D_{s2} + F(1 - P)], \quad (1)$$

where $P = \Sigma P_i \cdot D_i$ (P_i is weight fraction of a mineral "i" in the melting assemblage), F is the fraction of melting, and D_{s1} and D_{s2} are the bulk partition coefficients for stage 1 (metasomatism) and stage 2 (basalt generation), respectively. In this modeling, F is 0.03 (3% melting) and there are no phase exhaustion's over this melting range (all phases are residual). Element concentrations in the silicate liquid (stage 2) generated after metasomatism by a carbonatite- or silicate-liquid (stage 1) are illustrated as a function of concentration in the metasomatizing liquid (c_m) in Fig. 6b. In this manner, the effect of different D's on the composition of subsequent melts (stage 2) of mantle affected by small degree melts may be evaluated independently of trace element abundances in those small degree melts (stage 1) which are largely unknown.

Most obvious, is the relative enrichment in Na, Nb, Ta, Sr, Zr, Y, Lu, and Cr and relative depletions in K expected in a stage 2 silicate liquid which has been derived from a carbonatite metasomatized mantle relative to a silicate metasomatized mantle (Fig. 6b). The relative enrichment predicted for Zr, however, is dependent upon the D_{Zr} used for opx-silicate melt. In this model we have used a $D_{Zr}^{opx\text{-}silmelt}$ (0.03) determined by Ulmer (1989) which is in the range 0.003–0.18 of the available data (Fig. 4d). However, if a value at the higher end of this range is used (e.g., 0.18 from Green et al., 1989), then the relative enrichment of Zr in mantle affected by Zr is equal to that affected by carbonatite melts. Thus, excluding Zr as ambiguous until more data is available, the effect on inter element ratios by the two styles of metasomatism is assessed by considering ratios involving Ti, which is similar in abundance in melts derived from mantle affected by carbonatite or silicate metasomatism. Ti/Na, Ti/Y, Ti/Lu, Ti/Nb, Ti/Ta, and Ti/Sr would be lower in melts derived from source mantle affected by carbonatite metasomatism relative to melts derived from silicate metasomatized mantle (Fig. 6b). These ratios would also be lowered in a peridotite residue affected by carbonatite metasomatism relative to one affected by sili-

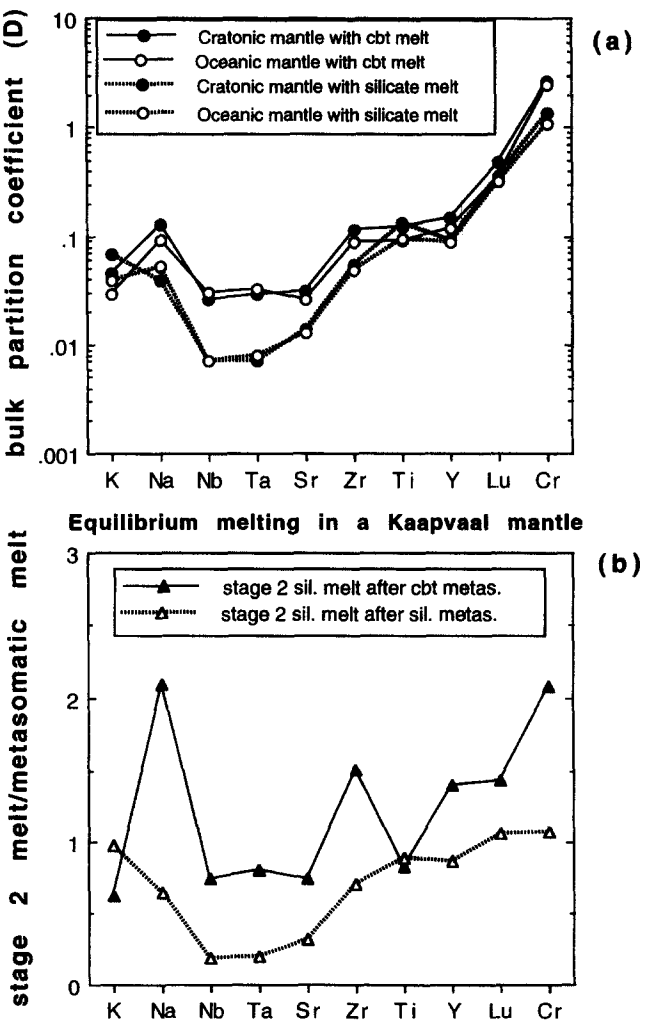

FIG. 6. (a) Bulk partition coefficients for a cratonic (e.g., Kaapvaal) lithospheric mantle peridotite and oceanic peridotite equilibrated with a carbonatite (cbt) and silicate (sil) melt. (b) Trace element abundances in melts (c_l) derived by equilibrium melting (stage 2) of a mantle which has undergone carbonatite or silicate metasomatism is divided by abundances in the stage 1 metasomatic melts (c_m). Explanation in text.

cate metasomatism (end of stage 1) as indicated by the relative bulk D's (Fig. 6a).

These numerical models have one simplifying assumption: in order to compare the effects of the different melts (silicate and carbonatite), the compositions in the stage 2 liquid (c_l) are presented relative to the abundances in the stage 1 metasomatic melt (c_m). Thus, for equal c_m in carbonatite and silicate metasomatic liquids, the processes are directly comparable (above discussion). The chemical influence of carbonatites would also be dependent on absolute element abundances in the metasomatic melts and this is assessed below using natural data.

6.2. Evidence for Carbonate Melts in the Mantle and Their Composition

Many recent studies have documented evidence for the interaction of carbonatite melts with peridotite xenoliths (Yaxley et al., 1991; Hauri et al., 1993; Ionov et al., 1993; Rudnick et al., 1993). In wehrlitic xenoliths from SE Australia, Yaxley et al. (1991) presented convincing evidence to show that the mineralogy (clinopyroxene-enriched character and the presence of pargasitic amphibole and apatite) was a consequence of carbonatite metasomatism. This major element evidence was correlated with high La/Yb, Zr/Hf, and Ca/Al ratios and low Ti/Eu ratios. Rudnick et al. (1993) pointed out that these ratio values are not individually unique to carbonatite melts (except perhaps Zr/Hf), but together provide evidence for carbonatite metasomatism. Rudnick et al. (1993) documented evidence for the interaction of carbonatite melt with peridotites from northern Tanzania. This included no orthopyroxene in some xenoliths (orthopyroxene + dolomitic melt = olivine + clinopyroxene), the presence of apatite and monazite, and high La/Yb, Nb/La, and Zr/Hf ratios and low Ti/Eu ratios. Ionov et al. (1993) examined carbonated xenoliths from Spitsbergen and correlated the interaction of carbonatite melt with increasing Sr/Sm, Sm/Hf, La/Nb, Zr/Hf, and Nb/Ta ratios. Hauri et al. (1993) documented the first evidence for carbonatite metasomatism in peridotites from an oceanic environment (Western Samoa and the Austral Islands). These peridotites contained a secondary assemblages of clinopyroxene + spinel ± apatite and bulk rocks had depletions of Ti, Zr, Nb, and Sr relative to the REEs. Hauri et al. (1993) used the trace element composition of clinopyroxenes and published carbonatite-clinopyroxene D's to determine the composition of putative carbonatite melts and these were characterized by depletions in Ti, Zr, and Nb relative to REEs. The trace element characteristics of these calculated carbonatite melts were quite similar to those reported by Nelson et al. (1988) for natural carbonatites, the only difference being that the calculated melts had high La/Nb values relative to continental carbonatite melts and Hauri et al. (1993) ascribed this to a characteristic of the oceanic mantle. In addition, there appears to be some ambiguity regarding the behaviour of La/Nb ratios (compare Rudnick et al., 1993 with Ionov et al., 1993). Comparison of natural carbonatite compositions (Nelson et al., 1988) with silicate melt compositions such as OIB (e.g., Sun and McDonough, 1989) shows carbonatites to be enriched in La, Ce, and Sr and depleted in Hf and Ti. Thus, the work on the natural sample (peridotites affected by carbonatites and carbonatites themselves) consistently predicts high LREE/HREE, LREE/Hf, and Sr/Hf ratios and low Ti/Sr and Ti/REE ratios in mantle mineralogies residual to carbonatite interaction. The partition coefficient data presented in this study supports the decrease in Ti/Sr and Ti/REE ratios in residual mantle mineralogies affected by carbonatite metasomatism suggested from the natural data. We cannot assess the effect on ratios involving Hf and the LREE/HREE fractionations with the current dataset.

7. SUMMARY OF CONCLUSIONS

The partitioning of selected trace elements between the major peridotite minerals (olivine, orthopyroxene, clinopyroxene, phlogopite) and carbonatite melt has been measured in this study. Data for clinopyroxene and garnet in equilibrium with carbonatite melt is similar to published data and not significantly different from published data for silicate melt partitioning (Fig. 4a,b). The D's for trace element partitioning between olivine- and orthopyroxene-carbonatite melt are elevated relative to published values for silicate melts (Fig. 4c,d). D's for phlogopite-carbonatite melt are less than or equal to published data for silicate melts, although the data are few. To test the likelihood of interelement fractionation in residual minerals between carbonatite- and silicate-melts, a model is examined supposing the generation of a second stage silicate melt from a mantle affected by small degree carbonatite- or silicate-melts in a first stage metasomatic event. In a second stage silicate melt all elements, except for K and Ti, will have elevated concentrations if the melt is derived from a mantle portion affected by carbonatite metasomatism vs. silicate melt metasomatism (Fig. 5b). This is a function of the greater D's for carbonatite melt with olivine and orthopyroxene which dominate the residue. In terms of interelement fractionations, Ti/Na, Ti/Y, Ti/Lu, Ti/Nb, Ti/Ta, and Ti/Sr ratios would be lower in melts derived from source mantle affected by carbonatite metasomatism relative to melts derived from silicate metasomatized mantle (Fig. 6b) and lower in a peridotite residual to such an event.

However, this model assumed equal abundances of the trace elements in the metasomatic (carbonatitic and silicate) melts to test the effect of D's independent of trace element concentrations in metasomatic melts. There is abundant natural evidence that this would not be the case: carbonatite melts have consistently greater abundances of LREEs and Sr and lower abundances of Ti and Hf relative to silicate melts. Absolute abundances in carbonatites suggests that LREE/HREE, LREE/Hf, and Sr/Hf ratios would increase and Ti/Sr and Ti/REE ratios would decrease in any peridotite affected by these melts. The partition coefficient data is consistent with these trends in the peridotite residue (i.e., a lowering of Ti/Sr, Ti/Lu, and Ti/Y ratios). Thus, increasing LREE/HREE, LREE/Hf, and Sr/Hf ratios and decreasing Ti/Sr and Ti/REE ratios in mantle mineralogies are unambiguous indicators of carbonate metasomatism.

Acknowledgments—Laboratory and analytical support from Peter Ulmer, Alan Thompson, and the staff of the Van de Graaff Group, National Accelerator Centre (South Africa) are gratefully acknowledged. M. Menzies, T. Green, D. Baker, and two anonymous reviewers are thanked for constructive comments. Jurgen Konzett and Peter

Ulmer are thanked for helpful comment on a draft version of the manuscript. Funding was provided by the Swiss National Science Foundation and the National Accelerator Centre (South Africa).

Editorial handling: M. Menzies

REFERENCES

Adam J. and Green T. H. (1994) The effects of pressure and temperature on the partitioning of Ti, Sr and REE between amphibole, clinopyroxene and basanitic melts. *Chem. Geol.* **117,** 219–234.

Blundy J. and Wood B. (1994) Prediction of crystal-melt partition coefficients from elastic moduli. *Nature* **372,** 452–454.

Boyd F. R. (1989) Compositional distinction between oceanic and cratonic lithosphere. *Earth Planet. Sci. Lett.* **96,** 15–26.

Boyd F. R. and England J. L. (1960) Apparatus for phase equilibrium measurements at pressures up to 50 kb and temperatures up to 1750°C. *J. Geophys. Res.* **65,** 741–748.

Dawson J. B. and Smith J. V. (1977) The MARID (mica-amphibole-rutile-ilmenite-diopside) suite of xenoliths in kimberlite. *Geochim. Cosmochim. Acta* **41,** 309–323.

Dalpe C. and Baker D. R. (1993) The importance of amphibole and mica in the generation of alkali basaltic suites. *Geol.-Min. Assoc. Canada, Prog. Abstr.* **A22.**

Deer W. A., Howie R. A., and Zussman J. (1966) *Rock-Forming Minerals.* Longman.

Gast P. W. (1968) Trace element fractionation and the origin of tholeiitic and alkaline magma types. *Geochim. Cosmochim. Acta* **32,** 1057–1086.

Green T. H. (1994) Experimental studies of trace-element partitioning applicable to igneous petrogenesis—Sedona 16 years later. *Chem. Geol.* **117,** 1–36.

Green T. H., Sie S. H., Ryan C. G., and Cousens D. R. (1989) Proton-microprobe determined partitioning of Nb, Ta, Zr, Y and Sr between garnet, clinopyroxene and basaltic melt at high pressure and temperature. *Chem. Geol.* **74,** 201–216.

Green T. H., Adam J., and Sie S. H. (1992) Trace element partitioning between silicate minerals and carbonatite at 25 kbar and application to mantle metasomatism. *Mineral. Petrol.* **46,** 179–184.

Guo J. and Green T. H. (1990) Experimental study of Barium partitioning between phlogopite and silicate liquid at upper-mantle pressure and temperature. *Lithos* **24,** 83–95.

Hart S. R. and Dunn T. (1993) Experimental cpx/melt partitioning of 24 trace elements. *Contrib. Mineral. Petrol.* **113,** 1–8.

Hauri E. H., Shimizu N., Dieu J. J., and Hart S. R. (1993) Evidence for hotspot-related carbonatite metasomatism in the oceanic upper mantle. *Nature* **365,** 221–227.

Ionov D. A., Dupuy C., O'Reilly S. Y., Kopylova G. M., and Genshaft Y. S. (1993) Carbonated peridotitic xenoliths from Spitsbergen: implications for trace element signature of mantle carbonate metasomatism. *Earth Planet. Sci. Lett.* **119,** 283–297.

Jenner G. A. et al. (1994) Determination of partition coefficients for trace elements in high pressure-temperature experimental run products by laser ablation microprobe-inductively coupled plasma mass spectrometry (LAM–ICP–MS). *Geochim. Cosmochim. Acta* **57,** 5099–5103.

Johnson K. T. M. (1994) Experimental cpx/ and garnet/melt partitioning of REE and other trace elements at high pressures: petrogenetic implications. *Mineral. Mag.* **58A,** 454–455.

Keller J. and Spettel B. (1995) The trace element composition and petrogenesis of natrocarbonatatites. In *Carbonatite Volcanism: Oldoinyo Lengai and the Petrogenesis of Natrocarbonatites* (ed. K. Bell and J. Keller); *IAVCEI Spec. Proc. Volcanol.* **4,** pp. 70–89.

Kennedy A. K., Lofgren G. E., and Wasserburg G. J. (1993) An experimental study of trace element partitioning between olivine, orthpyroxene and melt in chondrules: equilibrium values and kinetic effects. *Earth Planet. Sci. Lett.* **115,** 177–195.

Klemme S., Van Der Laan S., Foley S. F., and Gunther D. (1995) Experimentally determined trace and minor element partitioning between clinopyroxene and carbonatite melt under upper mantle conditions. *Earth Planet. Sci. Lett.* (in press).

Maaloe S. and Aoki K. (1977) The major element composition of the upper mantle estimated from the composition of lherzolites. *Contrib. Mineral. Petrol.* **76,** 127–147.

Mathias M., Siebert J. G., and Ringwood P. C. (1970) Some aspects of the mineralogy and petrology of ultramafic xenoliths in kimberlite. *Contrib. Mineral. Petrol.* **26,** 75–123.

Nelson D. R., Chivas A. R., Chappell B. W., and McCulloch M. T. (1988) Geochemical and isotopic systematics in carbonatites and implications for the evolution of ocean-island sources. *Geochim. Cosmochim. Acta* **52,** 1–17.

Onuma N., Higuchi H., Wakita H., and Nagasawa H. (1968) Trace element partition between two pyroxenes and the host lava. *Earth Planet. Sci. Lett.* **5,** 47–51.

Ringwood A. E. and Green D. H. (1966) An experimental investigation of the gabbro-eclogite transformation and some geophysical implications. *Tectonophys.* **3,** 383–427.

Rudnick R. L., McDonough W. F., and Chappell B. W. (1993) Carbonatite metasomatism in the northern Tanzanian mantle. *Earth Planet. Sci. Lett.* **114,** 463–475.

Ryan C. G. et al. (1990a) QuantitativePIXE microanalysis of geological materials using the CSIRO proton microprobe. *Nucl. Instr. Methods* **B47,** 55–71.

Ryan C. G., Cousens D. R., and Sie S. H. (1990b) Quantitative analysis of PIXE spectra in geoscience applications. *Nucl. Instr. Methods* **B49,** 271–276.

Shannon R. D. (1976) Revised effective ionic radii and systematic studies of interatomic distances in halides and chalcogenides. *Acta Crystall.* **A32,** 751–767.

Shaw D. M. (1970) Trace element fractionation during anatexis. *Geochim. Cosmochim. Acta* **34,** 237–243.

Sun S.-S. and McDonough W. F. (1989) Chemical and isotopic systematics of oceanic basalts: implications for mantle compositions and processes. In *Magmatism in the Ocean Basins* (ed. A. D. Saunders and M. J. Norry); *Geol. Soc. Spec. Pub.* **42,** 313–345.

Sweeney R. J. (1994) Carbonatite melt compositions in the Earth's mantle. *Earth Planet. Sci. Lett.* **128,** 259–270.

Sweeney R. J., Green D. H., and Sie S. H. (1992) Trace and minor element partitioning between garnet and amphibole and carbonatitic melt. *Earth Planet. Sci. Lett.* **113,** 1–14.

Sweeney R. J., Thompson A. B., and Ulmer P. (1993) Phase relations of a natural MARID composition and implications for MARID genesis, lithospheric melting and mantle metasomatism. *Contrib. Mineral. Petrol.* **115,** 225–241.

Sweeney R. J., Jablonski W., and Sie S. H. (1994) Determination of selected trace elements in silicates by electron and proton probe microanalysis. *X-ray Spectrom.* **23,** 91–95.

Tapper U. A. S. et al. (1993) High-brightness proton beams at the NAC nuclear microprobe. *Nucl. Instr. Methods* **B77,** 17–24.

Ulmer P. (1989) Partitioning of high-field strength elements among olivine, pyroxene, garnet and calc-alkaline picrobasalt: experimental results and an application. *Carnegie Inst. Wash. Yearb.* 1988–1989, 42–47.

Van Achterbergh E., Ryan C. G., Churms C. L., and Springhorn K. A. (1993) *Accuracy, Precision and Sensitivity of the Nuclear Microprobe; Annual Report NAC/AR/93-01.* National Accelerator Centre.

Walker D., Carpenter M. A., and Hitch C. M. (1990) Some simplifications to multi-anvil devices for high pressure experiments. *Amer. Mineral.* **75,** 1020–1028.

Wallace M. and Green D. H. (1988) An experimental determination of primary carbonatite composition. *Nature* **335,** 343–346.

Waters F. J. (1987) Suggested origin of MARID xenoliths in kimberlites by high pressure crystallization of an ultrapotassic rock such as lamproite. *Contrib. Mineral. Petrol.* **95,** 523–533.

Woolley A. R. and Kempe D. R. C. (1989) Carbonatites: Nomenclature, average chemical compositions and element distribution. In *Carbonatites—Genesis and Evolution* (ed. K. Bell), pp. 1–14. Unwin Hyman.

Yaxley G. M., Crawford A. J., and Green D. H. (1991) Evidence for carbonatite metasomatism in spinel peridotite xenoliths from western Victoria, Australia. *Earth Planet. Sci. Lett.* **107,** 305–317.